Geotechnical Aspects of Underground Construction in Soft Ground – Yoo, Park, Kim & Ban (Eds)

Numerical modelling of the interaction between a deep excavation and an ancient masonry wall

A. Amorosi
Technical University of Bari, Bari, Italy

D. Boldini
University of Bologna, Bologna, Italy

G. de Felice & M. Malena
University Roma Tre, Rome, Italy

G. Di Mucci
Metro C S.c.p.A, Rome, Italy

ABSTRACT: The city of Rome is currently involved in the construction of a new metro line, known as Metro C, which will underpass the historical city centre. This paper focuses on a 30 m deep excavation that will be constructed at short distance from the ancient masonry walls of the city, the Mura Aureliane at Porta Asinaria. A numerical investigation is here proposed to analyse the problem along a transversal section using the Finite Element code Plaxis. The Hardening Soil model is employed for the soil strata, while the masonry structure is schematised as an anisotropic elasto-plastic medium, whose properties are derived via homogenisation. The results indicate that the adopted engineering solutions for the supporting structure and the excavation sequence induce relatively small vertical and horizontal displacements in the ground and in the ancient wall, this latter being characterised by an almost rigid-body motion without significant damage induced in its masonry.

1 INTRODUCTION

Studies and research on the interplay between deep excavations and existing urban environment are becoming popular in relation to the large development of new transportation facilities. In the recent past a number of relevant scientific contributions focused on the prediction of the displacement field induced by excavations and the assessment of the related damage in surface structures (Mair & Taylor 1997).

The use of numerical methods to take into account the soil-structure interaction in this class of problems is nowadays common (e.g. Potts & Addenbrooke 1997, Liu et al. 2000, Son & Cording 2011, Amorosi et al. 2012, Amorosi et al. 2013). Nevertheless, the success of such analyses in practical application typically depends on the use of advanced constitutive models, on the ability to calibrate these models based on the experimental observations usually available is such engineering projects, and on the skill of the user in selecting the technical details and the significant construction stages which necessitate to be modelled in the analyses.

This paper focuses on a 30 m deep excavation that will be constructed at short distance from the ancient masonry walls of the city of Rome, the Mura Aureliane. This case history is assumed to be representative of the mutual interaction between architectural heritage and new infrastructures that crucially characterises the design and construction of underground infrastructures in historical city centers.

2 THE CASE STUDY

The new C line of the Rome subway, currently under construction, will have a total length of 25.5 km, connecting the North-West with the South-East side of the city, with 30 stations along its path. This study focuses on the deep excavation located between the stations San Giovanni and Piazza Venezia, that will be carried out at a very short distance (minimum 27 m) from the Mura Aureliane at Porta Asinaria (Figure 1).

The Mura Aureliane were built between 270 and 275 B.C. by Emperor Aurelio for defensive purposes, extending around the ancient city for about 19 km. Nowadays the wall is in a relatively good state of preservation for most of its current extension (12.5 km).

Porta Asinaria is one of the monumental access to the city, located in its south-eastern part, and it is characterised by a very well preserved state. In this area

Figure 1. View of the Mura Aureliane at Porta Asinaria (Metro C S.c.p.A. 2008).

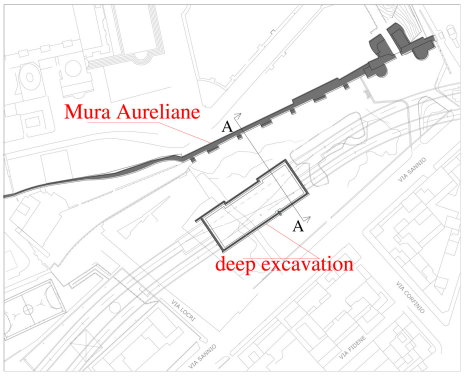

Figure 2. Plan view of the investigated area (A-A is the section of analysis).

the wall run from North-East to South-West, the subway under construction being located about parallel to it (Figure 2); the ground level behind the wall is at 45.3 m above sea level (a.s.l.), while that beyond it is at 34.5 m a.s.l.

The outer face of the wall is characterised by the presence of a series of buttresses, located at a regular distance. A schematic sketch of the wall is reported in Figure 3, which highlights its three layers section characterised by two external brick masonry leafs and the inner core filled with gravelly soil. The brick masonry of the walls was extensively restored in the 8th and 9th centuries, mainly in its upper parts, while the lower portions experienced some damage, characterised by large gaps in the brick veneer filled with mortar.

The geometry and mechanical properties of the masonry were investigated by means of in-situ and laboratory tests. More precisely, the transversal section was identified by means of drills and video-endoscopy, which allowed to characterise all the relevant geometrical data (external leaf thickness of about 95–115 cm, 200 cm wide inner core and internal leaf thickness of about 80–100 cm). Flat jack tests were also carried out to evaluate the masonry Young's modulus.

The excavation is $62.0 \times 23.7\,m^2$ large (the latter length reducing to 22.1 m in its central part). It will be

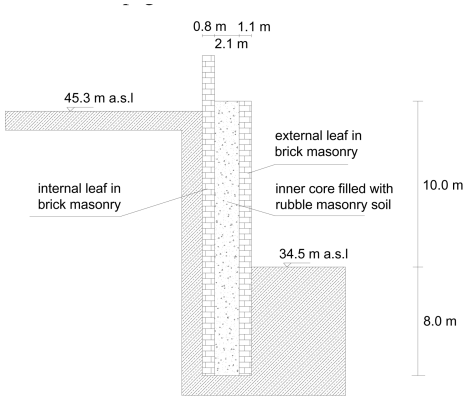

Figure 3. Geometry of the Mura Aureliane.

supported by 1.2 m thick concrete diaphragms having a length of 45 m. Internal horizontal support is provided by four slabs (the upper one, two intermediate ones and a base slab) which will be cast in place during the top-down excavation in order to improve the stability and to limit the disturbance to the adjacent masonry wall (Figure 4). A preliminary lowering of the piezometric level by draining wells, to be activated within the deep excavation site, will allow the construction sequence to be safely carried out.

The local subsoil consists of the following layers, starting from the ground surface:

- made ground (R), composed by coarse-grained material (sand and gravel in a fine grained pyroclastic matrix) with a thickness of about 15 m;
- alluvial deposits of the Tiber river (also known as LSO and St/Ar), constituted by silty sand, sandy silt and clayey silt of Holocene age, with a thickness of about 12 m;
- fluvial deposits (SG), made out of sand and gravel of Pleistocene age with a thickness of about 10 m;
- stiff overconsolidated clay of Pliocene age (Apl), which represents the bedrock of the city of Rome, for a thickness of hundreds of meters.

The hydraulic head is at about 26.0 m a.s.l. in the made ground layer and at about 17.5 m a.s.l. in the sand and gravel layer. The loss of hydraulic head is concentrated in the alluvial layer, characterised by a downward seepage flow.

3 NUMERICAL MODEL

The numerical model was set up using the commercial Finite Element code Plaxis 2D (2009). Figure 5 shows the analysed section, which was modelled by 15-node isoparametric elements for the soils and the masonry and 5-node beam elements for the structures.

The analysis was subdivided into several stages, all of which were performed assuming a drained response for all the strata (R, LSO-St/Ar and SG) except for the stiff Apl deep clay, which was considered undrained due to its relatively low permeability.

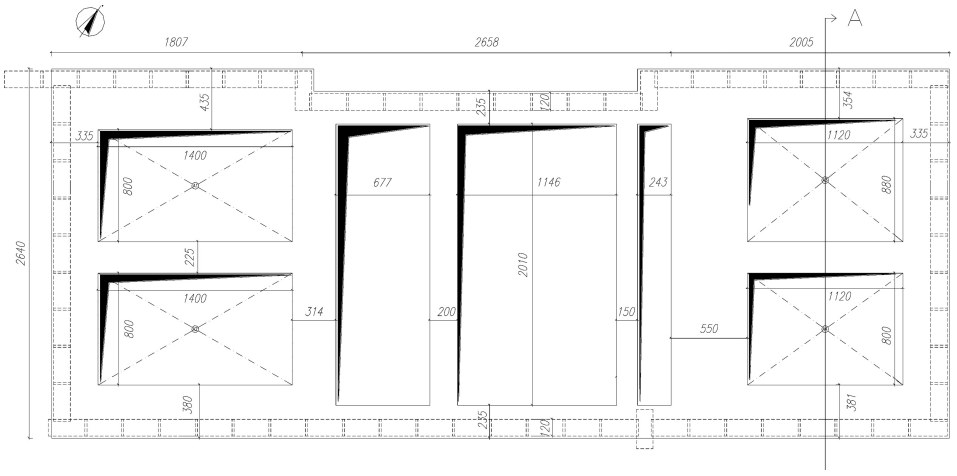

Figure 4. Detailed plan view of the upper slab (dimensions are given in centimetres).

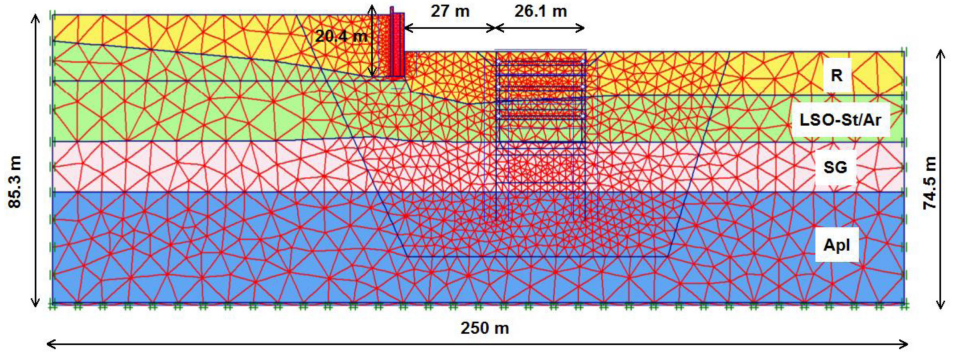

Figure 5. Sketch of the mesh (the geotechnical stratigraphy is also visible).

3.1 *Soil constitutive model*

The mechanical behaviour of the foundation strata is here described by the Hardening Soil model (HS), a constitutive law capable of taking into account the high soil stiffness observed at low strain, its variation with strain level and the early accumulation of plastic deformations (Schanz et al., 1999).

The elastic behaviour of the soil is defined by isotropic elasticity using a stress-dependent Young's modulus for unloading and reloading stress paths, which is a function of the effective stress and strength parameters according to the following expression:

$$E_{ur} = E_{ur}^{ref} \left(\frac{c' \cdot \cos\varphi' + \sigma'_3 \cdot \sin\varphi'}{c' \cdot \cos\varphi' + p^{ref} \cdot \sin\varphi'} \right)^m \qquad (1)$$

where E_{ur}^{ref} is the unloading-reloading Young's modulus at the reference pressure $p^{ref} = 100$ kPa, c' is the effective cohesion, φ' is the angle of shearing resistance, σ'_3 is the minimum principal effective stress and m is a constant that depends on the soil type. Similar expressions are used to define the secant stiffness in standard drained triaxial test, E_{50}, and the tangent stiffness for primary oedometer loading, E_{oed}.

The HS model is characterised by two yield surfaces which evolve isotropically: a shear hardening yield surface f_s that is a function of the deviatoric plastic strain and a cap yield surface f_v, which is introduced to bound the elastic region for compressive stress paths and depends on the plastic volumetric strain.

The elastic region of the models can be further reduced by means of a tensile cut-off.

The flow rule adopted for the cap yield surface f_v is associate while a non-associate flow rule is employed for the f_s, adopting a formulation inspired by the well-known stress-dilatancy theory by Rowe.

The geotechnical characterisation is based on the extensive investigation carried out in the area which included 10 boreholes, 10 Casagrande piezometers, 5 CPT tests, several SPT tests, 1 cross-hole test and a number of laboratory tests performed on the cohesive strata. Based on that, a consistent set of parameters was defined for each soil layer included in model (Table 1). The assumed values of *OCR* for the coarse-grained strata R and SG should to be considered fictitious,

Table 1. Geotechnical parameters of the different soil strata.

Soil layer	γ (kN/m^3)	c' (kPa)	φ' (°)	ψ (°)	ν_{ur} (–)	E_{ur}^{ref} (MPa)	m (–)	E_{50}^{ref} (MPa)	E_{oed}^{ref} (MPa)	OCR (–)	K_0 (–)	k (m/s)
R	17.0	5.0	31	0	0.20	143	1.0	14.3	14.3	3.5	1.000	1.0e–05
LSO-St/Ar	19.5	0.1	32	0	0.20	256	1.0	21.3	21.3	1.3	0.536	1.0e–06
SG	20.0	0.1	40	0	0.20	900	0.4	90.0	90.0	7.5	0.357	1.0e–05
Apl	21.0	40.0	26	0	0.20	450	0.9	22.5	22.5	2.5	0.840	1.0e–10

as their only scope is that of excluding yielding on the cap surface, while those defined for the cohesive strata were realistically determined from oedometer tests. For the sake of simplicity, the dilatancy parameter ψ is assumed null for all the materials.

3.2 *Masonry model*

The two external masonry leaves of the ancient wall were schematised by a regular and periodic assembly of bricks interacting through non-linear mortar joints (Figure 6).

The anisotropic strength criterion proposed by de Buhan & de Felice (1997) for periodic masonry, once reformulated into a continuum model as discussed in de Felice et al. (2010), was used after its implementation into the code Plaxis 2D. The original model, which results from a homogenization process based on the yield design theory, depends on the stiffness and strength of the constitutive material: joints are assumed to behave following a frictional Mohr–Coulomb criterion, depending on the friction angle ϕ and on the cohesion c of mortar and/or mortar-to-brick interface, the bricks being considered as infinitely resistant.

This strength domain is defined in the context of multi-surface perfect plasticity as:

$$E_\sigma = \left\{ \boldsymbol{\sigma} \mid f^\alpha(\boldsymbol{\sigma}) := \mathbf{n}^\alpha : \boldsymbol{\sigma} - c^\alpha \le 0 \ \forall \alpha \in \left[1,..,n_p\right] \right\} \quad (2)$$

where $f^\alpha(\boldsymbol{\sigma})$ are n_p independent planes, intersecting in a non-smooth way, which define the yield surface. In particular, the yield surface comprises $n_p = 4$ planes which can be written in terms of stress components in the Oxz reference adopted for the joints as follows:

$$\begin{aligned} &f^1 := m\sigma_{xx} + tg(\varphi)\sigma_{zz} + \left(1 + tg(\varphi)m\right)\sigma_{xz} + \\ &-c - cm / tg(\varphi) \le 0 \\ &f^2 := m\sigma_{xx} + tg(\varphi)\sigma_{zz} - \left(1 + tg(\varphi)m\right)\sigma_{xz} + \\ &-c - cm / tg(\varphi) \le 0 \\ &f^3 := \sigma_{zz} + 1/tg(\varphi)\sigma_{xz} - c/tg(\varphi) \le 0 \\ &f^4 := \sigma_{zz} - 1/tg(\varphi)\sigma_{xz} - c/tg(\varphi) \le 0 \end{aligned} \quad (3)$$

where $m = 2a/b$ is the aspect ratio height-to-width of the bricks.

The selected parameters a, b, c and ϕ are summarised in Table 2.

For both the masonry and the inner core filled with soil (this latter modelled as a linear elastic-perfectly plastic material), the unit weight of volume γ was assumed equal to 16 kN/m^3.

Figure 6. Masonry texture.

Table 2. Parameters for the wall materials.

	a (cm)	b (cm)	γ (kN/m^3)	E (MPa)	c (kPa)	φ (°)
Masonry	4	15	16.0	2400	50	30
Core	–	–	16.0	300	50	35

The elastic modulus of the masonry is equal to $E = 2400$ MPa according to the flat jack tests results, while the mechanical characteristics of the inner filled core are $E = 300$ MPa, $c = 50$ kPa, $\varphi = 35°$, based on the compression tests performed on the core samples retrieved by drilling.

3.3 *Scheme and parameters of the reinforced concrete structural elements*

The 1.2 m thick concrete diaphragms supporting the excavation were modelled by beam elements whose parameters are reported in Table 3.

The 2D modelling of the problem under study required some simplifications to be introduced with reference to the upper and intermediate slabs (Figure 4). In fact, the presence of openings in the slabs was accounted for by adopting continuous beam elements characterised by axial and flexural stiffness equivalent to the real one. The equivalent thickness was evaluated assuming the slab to be composed by 4 beams in series (all around the opening along section A-A) whose axial and/flexural stiffness were determined based on their geometrical characteristics, assuming for the reinforced concrete a Young's modulus of 30 GPa (Table 3).

Attached to each side of all the beam elements is an interface, to allow relative displacements to occur

Table 3. Characteristics and parameters of the beam elements used in the numerical analysis.

Structural element:	s (m)	γ (kN/m^3)	E (GPa)	ν (–)
Diaphragm	1.200	25.0	30	0.15
Upper and first intermediate slabs	0.475	–	30	0.15
Second intermediate slab	0.214	–	30	0.15

upon mobilisation of the adjacent soil's shear strength. In addition, a hinge connection was adopted between the diaphragms and upper and intermediate slabs.

For what concerns the base slab, which is continuous (i.e. no openings), its effective dimensions were adopted in the model ($s = 1.8$ m) (Table 3). Both base slab and the internal lining were simulated by non-porous elements adopting an elastic constitutive law characterised by $\gamma = 25.0$ kN/m^3, $\nu = 0.15$ and $E = 25$ GPa.

3.4 *Simulation of excavation*

The simulation of the staged construction of the deep excavation was modelled in detail, subdividing it as follows:

- initialisation of the lithostatic state of stress and of the initial hydraulic conditions with reference to the pre-construction site configuration;
- activation of the beam elements representing the diaphragm wall (from 30.5 to −14.5 m a.s.l.);
- lowering of the piezometric surface inside the diaphragm walls to −4.0 m a.s.l. and calculation of the new pore pressure distribution due to the seepage process;
- simulation of the unsupported excavation from the ground surface to the head of the diaphragm walls (a slope inclination angle of 45° was considered);
- activation of the beam elements representing the upper portion of the supporting system (from 30.5 to 31.7 m a.s.l., in continuity with the diaphragm walls);
- activation of the beam element representing the upper slab at 31.7 m a.s.l.;
- excavation from 30.5 to 27.5 m a.s.l.;
- excavation from 27.5 to 23.1 m a.s.l.;
- activation of the beam element representing the first intermediate slab at 24.3 m a.s.l.;
- excavation from 23.1 to 20.1 m a.s.l.;
- activation of the volume elements representing the internal lining between and upper and the first intermediate slabs;
- excavation from 20.1 to 17.4 m a.s.l.;
- excavation from 17.4 to 14.4 m a.s.l.;
- activation of the beam element representing the second intermediate slab at 15.4 m a.s.l. and activation of the volume elements representing the internal lining between and first and the second intermediate slabs;

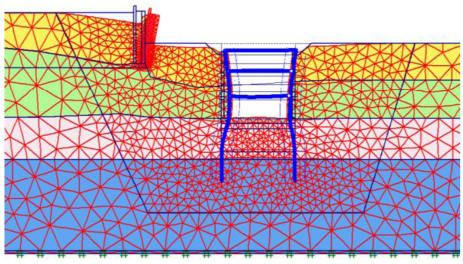

Figure 7. Deformed configuration of the mesh at the end of the analysis (magnification factor = 100).

- excavation from 14.4 to 8.1 m a.s.l.;
- excavation from 8.1 to 4.2 m a.s.l.;
- activation of the volume elements representing the lower slab (from 4.2 to 6.0 m a.s.l.) and activation of the elements representing the internal lining between the second intermediate and the lower slabs;
- retrieval of the initial hydraulic conditions and consolidation analysis.

4 NUMERICAL RESULTS

Figure 7 shows the deformed configuration of the mesh at the end of the analysis. It is possible to observe that the wall suffers a rotation as well as a right-downward translation due to the construction of the deep excavation. As expected, the displacements are less severe on the right side of the excavation.

Settlements and horizontal displacements at the ground surface (34.5 m a.s.l.) and at the foundation level of the wall (27.3 m a.s.l.) are shown in Figure 8. The graphs indicate that maximum horizontal displacements are larger than vertical ones, with differential settlements being rather concentrate under the wall. This latter structure undergoes a maximum settlement of about 14 mm together with a rightward horizontal displacement of about 16 mm.

The predicted plastic points in the soil layers are represented in Figure 9, which clearly indicates the kinematics of the wall as fully controlled by the underlying soil behaviour, this latter being characterised by the localisation of plastic shear strains along a plane which extends from the wall foundation down to the deeper portion of the adjacent diaphragm wall. No plastic deformations were indeed computed in the ancient wall.

A further analysis was then carried out assuming, as an extreme case, a reduction in the strength characteristics of the wall due to severe degradation phenomena. In particular, the cohesion of the masonry mortar joints c was reduced to 5 kPa while the corresponding friction angle φ was kept equal to 30°. The resulting tensile plastic strains obtained at the end of the analysis are plotted in Figure 10. They cumulate on the internal masonry leaf and reach a maximum value of 0.2%,

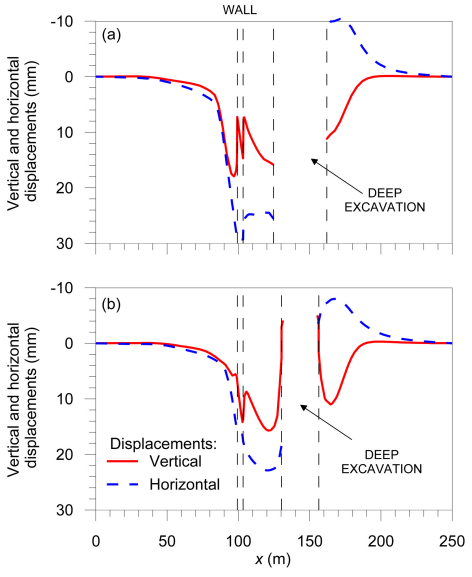

Figure 8. Settlements and horizontal displacements at the end of the analysis computed at the ground surface (a) and at the wall foundation level (b).

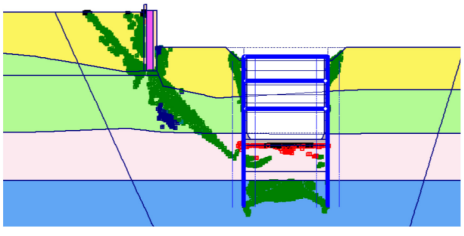

Figure 9. Distribution of plastic points at the end of the analysis (green and blue symbols represent cap and shear hardening plastic points, respectively; red symbols represent Mohr-Coulomb strength points).

thus indicating the occurrence of a moderate, though concentrated, damage.

5 CONCLUSIONS

The paper proposes a combined structural and geotechnical analysis, where the interaction between a historical wall and a nearby deep excavation is assessed by a 2D numerical approach, employing advanced constitutive models for both the soil and the wall masonry.

The results indicate that the adopted engineering solutions for the supporting structure and the excavation sequence induce relatively small vertical and horizontal displacements in the ground surrounding the excavation and in the ancient wall. The overall picture indicates that the portion of Mura Aureliane interacting with the excavation is subjected to a prevailing rigid motion that preserves it from any damage along the transversal section under study.

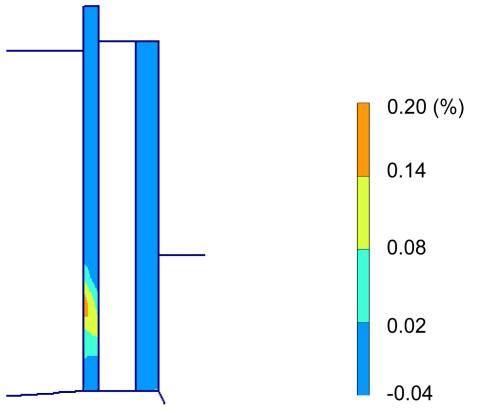

Figure 10. Distribution of tensile plastic strains in the masonry wall at the end of the analysis considering a degradation of the wall strength parameters.

A worst scenario analysis, carried out assuming a significant, though not realistic, degradation phenomena for the wall, indicates that moderate damage would occur in the internal masonry leaf of the wall. Possible damage, not investigated here, might stem from the differential movements of the wall along its longitudinal extension, due to the limited dimension of the deep excavation. In order to detect this latter pattern of behaviour, a 3D analysis should be carried out, representing the next step of this research activity.

REFERENCES

Amorosi, A., Boldini, D., de Felice, G. & Malena, M. (2012). Tunnelling-induced deformation in a masonry structure: a numerical approach. *7th Int. Symp. on Geotech. Aspects of Underground Construction in Soft Ground*, 353–359.

Amorosi, A., Boldini, D., de Felice, G., Malena, M. & Sebastianelli, M. (2013). Tunnelling-induced deformation and damage on historical masonry structures. *Géotechnique*: 64(2), 118-130.

de Buhan, P. & de Felice, G. (1997). A homogenisation approach to the ultimate strength of brick masonry. *J. Mech. Phys. Solids*: 45(7), 1085–1104.

de Felice, G., Amorosi, A. & Malena, M. (2010). Elasto-plastic analysis of block structures through a homogeneization method. *Int. J. Numer. Analyt. Methods Geomech.*: 34(3), 221–247.

Liu, G., Houlsby, G. T. & Augarde, C. E. (2000). 2-dimensional analysis of settlement damage to masonry buildings caused by tunnelling. *The Struct. Engr*: 79(1), 19–25.

Metro C S.c.p.A. (2008). *Progetto Definitivo*.

Plaxis 2D (2009). Reference manual. Version 9.0.

Potts, D. M. & Addenbrooke, T. I. (1997). A structure's influence on tunnelling-induced ground movements. *Proc. Instn Civ. Engrs – Geotech. Engng*: 125(2), 109–125.

Schanz, T., Vermeer, P. A. & Bonnier, P. G. (1999). The hardening soil model: formulation and verification. *Conf. Beyond 2000 in Computational Geotechnics,* 1–16.

Son, M. & Cording, E. J. (2011). Responses of buildings with different structural types to excavation-induced ground settlements. *J. Geotech. Geoenviron. Engng*: 137(4), 323–344.